SPE-200469-MS

Feasibility Study of Gas Injection in Low Permeability Reservoirs of Changqing Oilfield

Ye Tian, Ozan Uzun, and Yizi Shen, Colorado School of Mines; Zhengdong Lei, Jiangru Yuan, and Jiaheng Chen, Research Institute of Petroleum Exploration and Development, PetroChina; Hossein Kazemi and Yu-Shu Wu, Colorado School of Mines

Copyright 2020, Society of Petroleum Engineers

This paper was prepared for presentation at the SPE Improved Oil Recovery Conference originally scheduled to be held in Tulsa, OK, USA, 18 – 22 April 2020. Due to COVID-19 the physical event was postponed until 31 August – 4 September 2020 and was changed to a virtual event. The official proceedings were published online on 30 August 2020.

This paper was selected for presentation by an SPE program committee following review of information contained in an abstract submitted by the author(s). Contents of the paper have not been reviewed by the Society of Petroleum Engineers and are subject to correction by the author(s). The material does not necessarily reflect any position of the Society of Petroleum Engineers, its officers, or members. Electronic reproduction, distribution, or storage of any part of this paper without the written consent of the Society of Petroleum Engineers is prohibited. Permission to reproduce in print is restricted to an abstract of not more than 300 words; illustrations may not be copied. The abstract must contain conspicuous acknowledgment of SPE copyright.

Abstract

Changqing Oilfield is the largest petroleum-producing field in China and one-third of its oil production is attributed to the formations with permeability lower than 1 mD. The rapid oil rate decline and low recovery factor (RF) associated with those formations require additional IOR/EOR measures besides waterflood. Based on the promising results from recent gas injection pilots in North America, we investigated the feasibility of gas injection in the low permeability formation (Chang 6_3) of Changqing Oilfield.

An eight-component fluid characterization, which fits both the constant composition expansion (CCE) test and separator test, was used in a numerical dual-porosity compositional model. A typical well pattern, composed of six vertical injectors and one horizontal producer, is selected for the modeling study. The input parameters, including relative permeability, fracture permeability, etc., were adjusted to achieve an acceptable history match of the production data. Huff-n-Puff using several gases—lean gas (CH_4), produced gas, rich gas (C_2H_6), and solvent (C_3H_8)— were investigated and the results were compared with the current waterflood.

The simulation results show that the richer the injected gas, the higher the oil production. C_3H_8 huff-n-puff achieved the best performance, increasing the cumulative oil production by a factor of 2.28 after 5 cycles, then followed by C_2H_6 as 1.34, produced gas as 1.08. CH_4 alone demonstrated a lower recovery factor than waterflood, because its minimum miscibility pressure (MMP) is close to the maximum allowable injection pressure, i.e., the minimum horizontal stress. In addition, the horizontal producer was completed at the reservoir top and water injectors were placed at the bottom, which was originally designed to improve the waterflood by gravity segregation. Under such well placement design, the miscible oil bank, which forms at the injection front during vaporizing drive, will be displaced towards the reservoir bottom even out of the SRV, undermining the huff-n-puff performance. Injection with rich gas will be more compatible, as the miscible bank forms at the injection tail. Injecting produced gas enriched with C_3H_8 will hence achieve promising EOR performance. The simulation also shows that increasing injection pressure increases the recovery factor. The leaner composition of produced gas could be compensated by a higher injection

Downloaded from http://onepetro.org/SPEIOR/proceedings-pdf/20IOR/2-20IOR/D021S023R001/2369981/spe-200469-ms.pdf by Colorado School of Mines user on 12 September 2021

pressure. The optimal injection duration and soaking time could also be obtained after sensitivity analysis. Another critical factor is the fracture network characterized by the dual-porosity model, as simulation with the single porosity model only shows minor improvement in RF even with C_3H_8.

Our work confirmed the technical feasibility of injecting rich gas in the low permeability Chang 6_3 by compositional simulation. We also determined the key parameters for the operator to consider in the next phase of the project.

Introduction

Changqing Oilfield located in the Ordos Basin is the largest oil and gas producing field in China and produced about 57 million tonnes of oil equivalent in 2019 (1.15 million barrels of oil equivalent daily). The Changqing Oilfield Company, a subsidiary of PetroChina, first started its production in the 1970s from Jurassic formations with relatively good properties, where permeability ranges from 10 to 100 mD (Liu et al., 2012; Yu et al., 2019). In recent years, production from these formations gradually became uneconomical; therefore, low-permeability and ultra-low permeability Triassic formations have emerged as the main target of development (Shangguan et al., 2015).

The subject of this study is the Y284 Unit and its main producing layers lie in the third sub-member of the sixth member of the upper Triassic Yanchang formation (also known as Chang 6_3), which contains green-greyish siltstones with dark grey mud intercalation (Shi, 2012). The average air permeability without confining pressure is estimated as 0.38 mD. The main producing interval is Chang 6_3^1, which is a continuous sand body at the top of Chang 6_3 with the average thickness as 21.2 m, porosity as 12.1% and initial oil saturation as 55%. 756 producers were deployed in the Y284 Unit by the end of 2017 (Xin, 2019) and can be classified into two categories: fractured vertical wells and fractured horizontal wells. Waterflood with 384 vertical injectors was implemented in this reservoir at the start of or even prior to production in order to compensate for the low initial reservoir pressure, which is a common practice in Changqing (Ran et al., 2013). Most vertical wells are in the diamond inverted nine-spot pattern, with extended well spacing along the direction of maximum horizontal stress in order to delay water breakthrough along natural fractures and improve sweep efficiency as circled by the black long dash line in Figure 1. The average oil production rate per vertical well was 1.47 m^3/d and the average water-cut was 51.6% in 2017. The earliest production with vertical wells started in 2005. Horizontal wells with 6-8 fracture stages lie in the rectangular five-spot pattern as circled by the green short dash line in Figure 1. The average oil rate per well was 0.87 m^3/d and the average water-cut was 64.1% in 2017 after 7 years of production. Horizontal wells with average 8 hydraulic fracture stages lie at the center of the rectangular seven-spot pattern as circled by the yellow line in Figure 1. The average oil rate per well was 3.08 m^3/d and the average water-cut was 32.5% as most of the horizontal wells started production after 2012. Judging from the daily oil rate and water-cut, horizontal wells in the seven-spot pattern seem to have the best performance followed by vertical wells in the inverted nine-spot and horizontal wells in the five-spot pattern. However, the performance of waterflood in this unit is deemed as unsatisfactory and effective displacement has not been established, resulting in a very low oil rate and lower than expected recovery factor. Early reservoir simulation studies predicted different ultimate recovery factors for example 10% (Dong, 2015), 15% (Zhao et al., 2015) after waterflood in the horizontal-well-developed region. But the actual recovery factor till 2017 was much lower than expected. Hence, improved/enhanced oil recovery (IOR/EOR) methods beyond waterflood is desired.

Based on the favorable results from recent gas injection pilots in North America (Wang et al., 2017), gas injection seems to be a promising option for ultra-low permeability reservoirs, especially when developed by multistage hydraulic fractured horizontal wells (Atan et al., 2018; Zhang et al., 2019). A region which contained all three typical patterns as circled by the blue lines in Figure 1, was hence selected by the operator for pilot IOR/EOR studies.

Downloaded from http://onepetro.org/SPEIOR/proceedings-pdf/20IOR/2-20IOR/D021S023R001/2369981/spe-200469-ms.pdf by Colorado School of Mines user on 12 September 2021

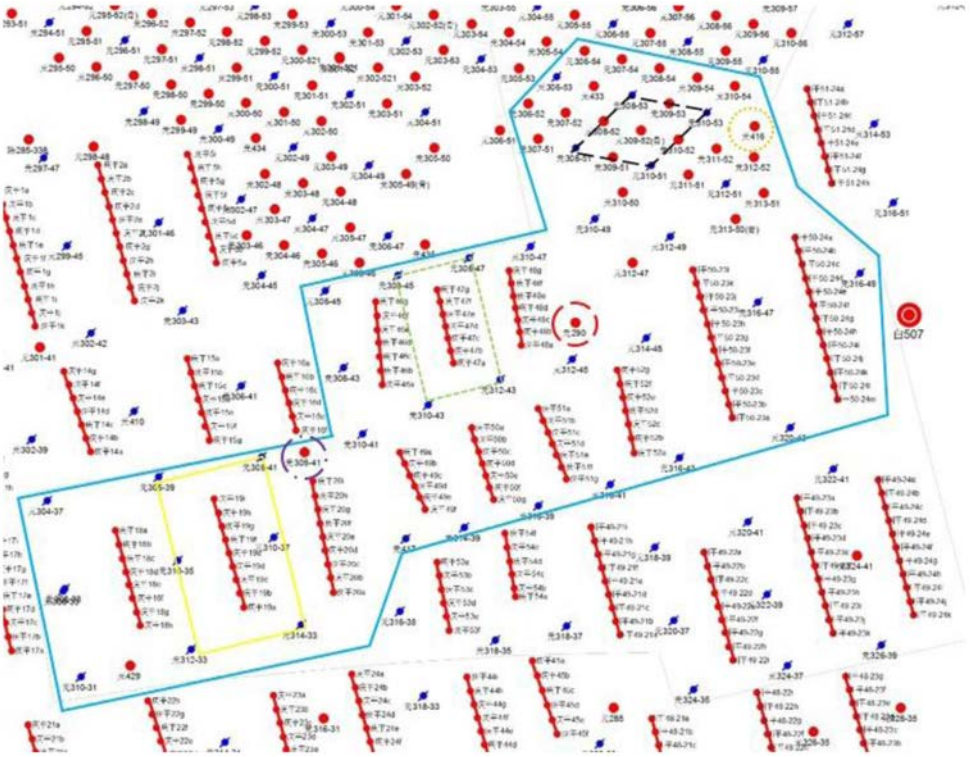

Figure. 1—Boundaries of the pilot region within the Y284 Unit

The pilot region was first investigated by Hu (2018) using a black oil model as shown in Figure 2. The grid size was 25 m in both I and J direction. And there were 15 vertical layers with total thickness as 75 m. And the total grid number was 691,650 before refinement. The model was rotated 15 degrees counterclockwise in the IJ plane, making I direction parallel to the direction of maximum horizontal stress as NE75°. Such rotation aimed at simplifying the fracture modeling as logarithmic local refinement was then only needed in J direction. After grid refinements, the total grid became 711,540. The initial reservoir pressure was 15.8 MPa and the temperature was 69.7 °C at the mid-depth of the reservoir.

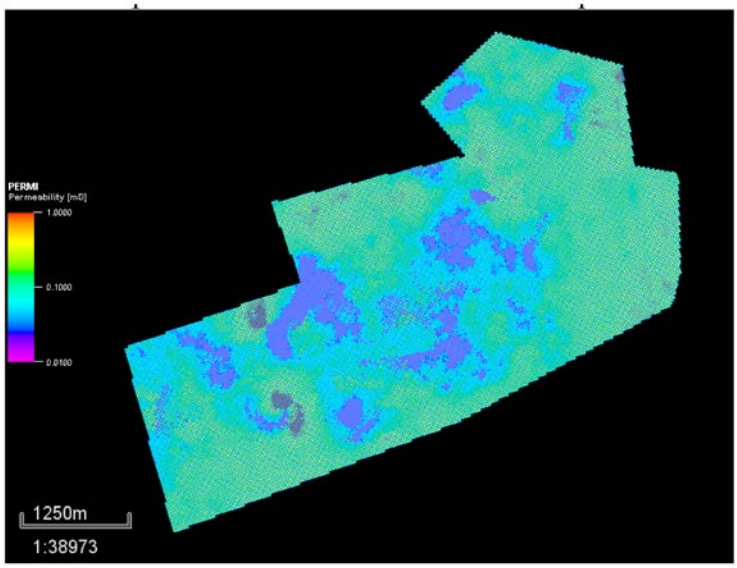

Figure. 2—The full-field model of the pilot region built by Hu (2018)

Downloaded from http://onepetro.org/SPEIOR/proceedings-pdf/20IOR/2-20IOR/D021S023R001/2369981/spe-200469-ms.pdf by Colorado School of Mines user on 12 September 2021

The major issue with the previous black oil model was its poor history matching. With the total liquid rate as the history matching constraints, the oil rate was qualitatively matched. But there were apparent discrepancies with respect to the bottom hole pressure (BHP). The actual BHP (measured by bottomhole pressure gauge from Aug 2016 to Sep 2016) was 5.2 MPa, much lower than the calculated BHP as 13.4 MPa from the black oil model as shown in Figure 3. Reservoir properties including rock permeability, fracture conductivities, relative permeability curves should be carefully tuned to match the water cut and BHP during the waterflood to improve the model's reliability.

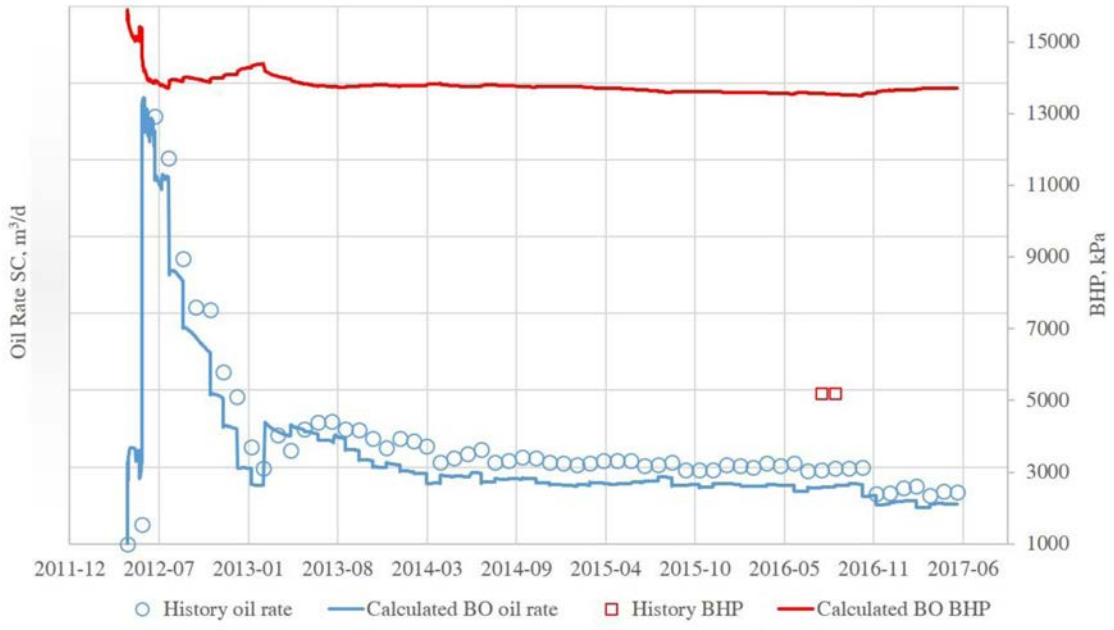

Figure. 3—Poor history-matching performance of Well QP19 by the previous black oil model

Moreover, since the black oil model is no longer valid when the transport process is strongly composition-dependent during gas injection, it should be replaced by a compositional model to improve the simulation accuracy (Tian et al., 2019). Hence, an equation-of-state (EOS) based compositional model was used to investigate the viability of gas injection in the Chang 6_3 formation of Changqing Oilfield.

Compositional modeling

Running a full-field compositional model takes a significantly longer time than the black oil model due to the increased number of governing equations as well as costly phase equilibrium calculations. To reduce the computational cost, a typical well pattern QP19 was subtracted from the pilot region (circled by the yellow solid line in Figure 1) and compositionally modeled as shown in Figure 5. The initial water saturation, reservoir pressure, and grid geometry were the same as the full field model. There were 38,320 grids in the sub-model with 39 grids in I direction, 61 grids in J direction, and 15 grids in J direction. There were seven wells in the sub-model including one fractured horizontal producer (QP19) and six water injectors (Y306-39, Y308-41, Y310-35, Y310-37, Y312-33, Y314-33). The water injection rate was proportionally scaled based on the well location, i.e., a factor of 1/4 for the injector at the corner (e.g., Y306-39) and a factor of 1/2 for the injector on the side (e.g., Y310-35). QP19 was perforated at the top of the reservoir and completed with 8 hydraulic fractures whose half-length ranged from 150 to 175 m in I direction and height ranged from 8-16 m in J direction. Water injectors injecting below the formation breakdown pressure were placed at the lower part of the reservoir, which was originally designed to improve the sweep efficiency of waterflood by gravity.

Downloaded from http://onepetro.org/SPEIOR/proceedings-pdf/20IOR/2-20IOR/D021S023R001/2369981/spe-200469-ms.pdf by Colorado School of Mines user on 12 September 2021

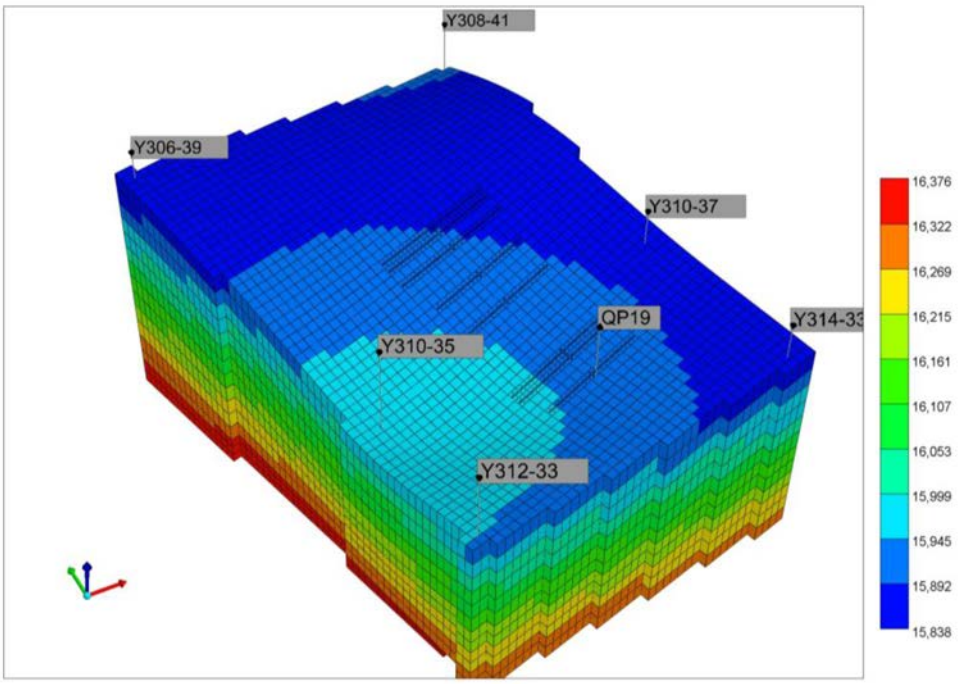

Figure. 4—A typical well pattern subtracted from the full-field model

In the following subsection, critical fluid and rock properties were meticulously re-calibrated and tuned based on experimental results and history matching in order to provide reliable inputs for the subsequent compositional simulation.

Reservoir fluid characterization

The reservoir fluid was sampled and tested in 2010 from producer Y309-41, whose location is circled by the purple long dash dot line in Figure 1. Downhole sampling was carried out at a pressure of 13.501 MPa which was higher than the saturation pressure as 13.087 MPa. The fluid sample then underwent constant composition expansion (CCE) test, one-stage separator test and viscosity measurement at various pressure and constant reservoir temperature in a commercial laboratory. The overall molar composition of the fluid was listed in Table 1 with respect to 15 carbon number groups.

Table 1—Overall composition of the reservoir fluid

Component	N_2	CO_2	C1	C2	C3	iC4	nC4	iC5	nC5	C6	C7	C8	C9	C10	C11+
molar fraction, %	0.75	0.12	31.72	8.35	9.70	1.49	4.62	1.62	2.25	2.84	3.24	4.49	2.88	2.25	23.67

For the practical compositional simulation purpose, we then lumped the 15 components in the original PVT laboratory report into 8 pseudo components in WinProp including CO_2, N_2, CH_4, C_2H_6, C_3H_8, C4-6, C7-10, C11+. Because of CO_2 and N_2's possibility as injectants, they were still listed as an individual component despite their low fractions. C7+ was split into two pseudo components, i.e., C7-10 and C11+ based on the molar fraction of C7+ (Khan, 1992). Then the binary-interaction coefficients (BIC) between pure components (especially CH_4) and pseudo-components were first tuned to match the bubble point pressure as shown in Figure 5. The volume shift parameters, critical pressure, and critical temperature of pseudo-components were then tuned to match the oil density from the CCE test as shown in Figure 6. Viscosity parameters including critical volume, mixing rule exponent, and polynomial coefficients in Jossi-Stiel-Thodos correlation were subsequently tuned to match oil viscosities at different pressure as shown in

Downloaded from http://onepetro.org/SPEIOR/proceedings-pdf/20IOR/2-20IOR/D021S023R001/2369981/spe-200469-ms.pdf by Colorado School of Mines user on 12 September 2021

Figure 7. The calculated gas-oil ratio at reservoir condition with separator condition as 20 °C and 1 atm is 120.10 m^3/m^3, close to the measured value as 120.12 m^3/m^3. The calculated stock oil density for oil is 832.5 kg/m^3 matching the experimental value as 832.5 kg/m^3.

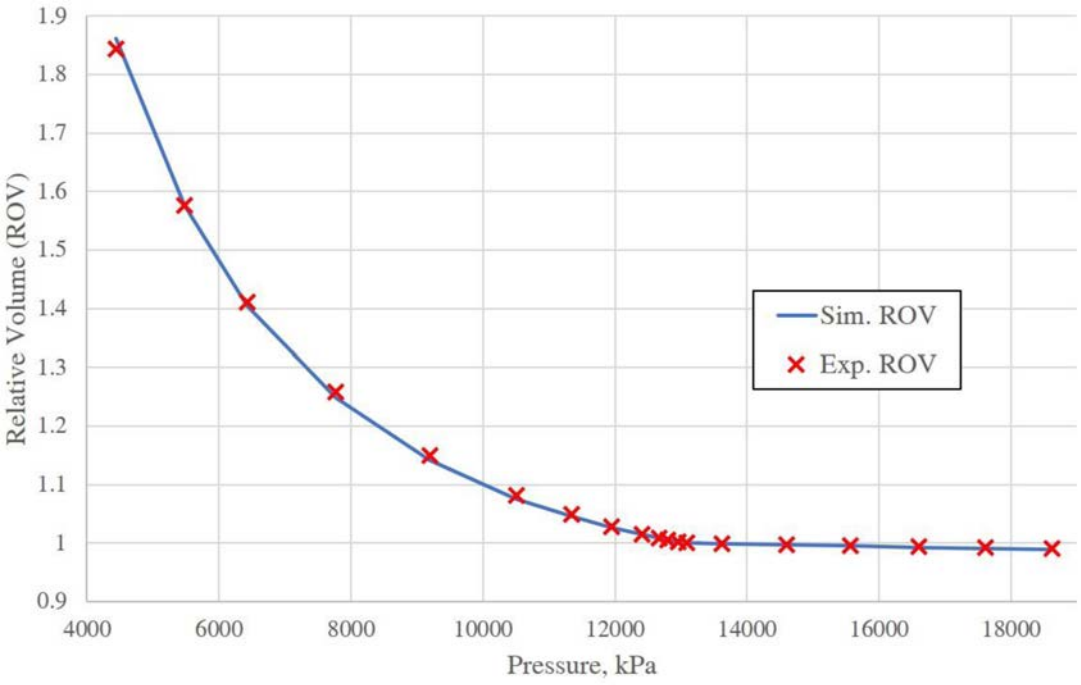

Figure. 5—Matched relative volume and bubble point pressure

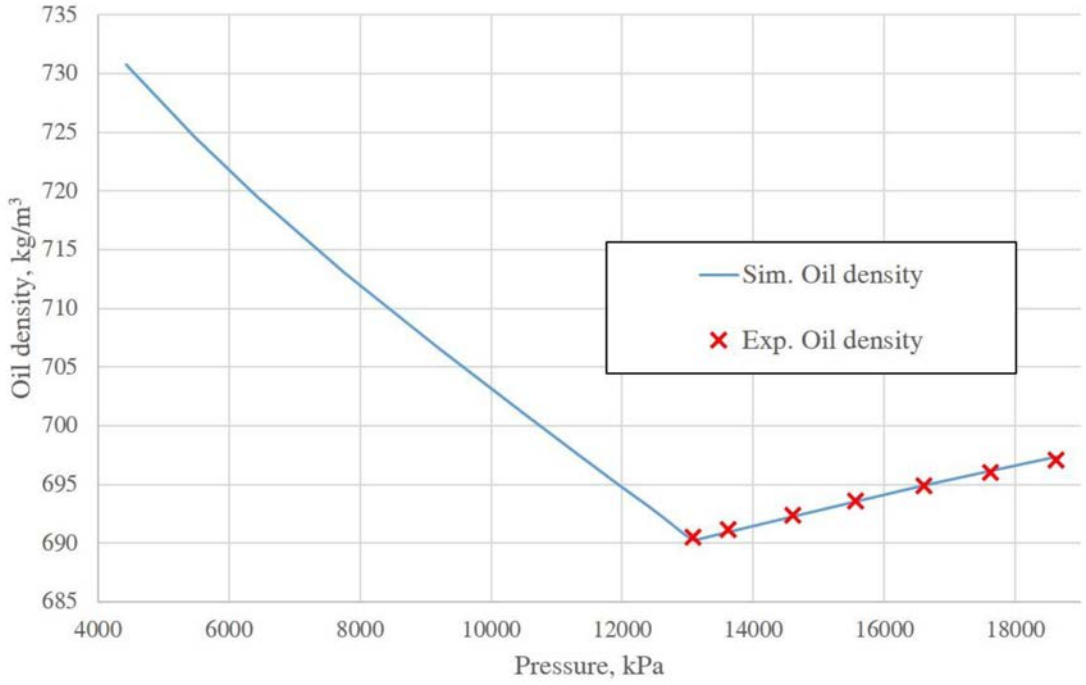

Figure. 6—Matched oil density

Downloaded from http://onepetro.org/SPEIOR/proceedings-pdf/20IOR/2-20IOR/D021S023R001/2369981/spe-200469-ms.pdf by Colorado School of Mines user on 12 September 2021

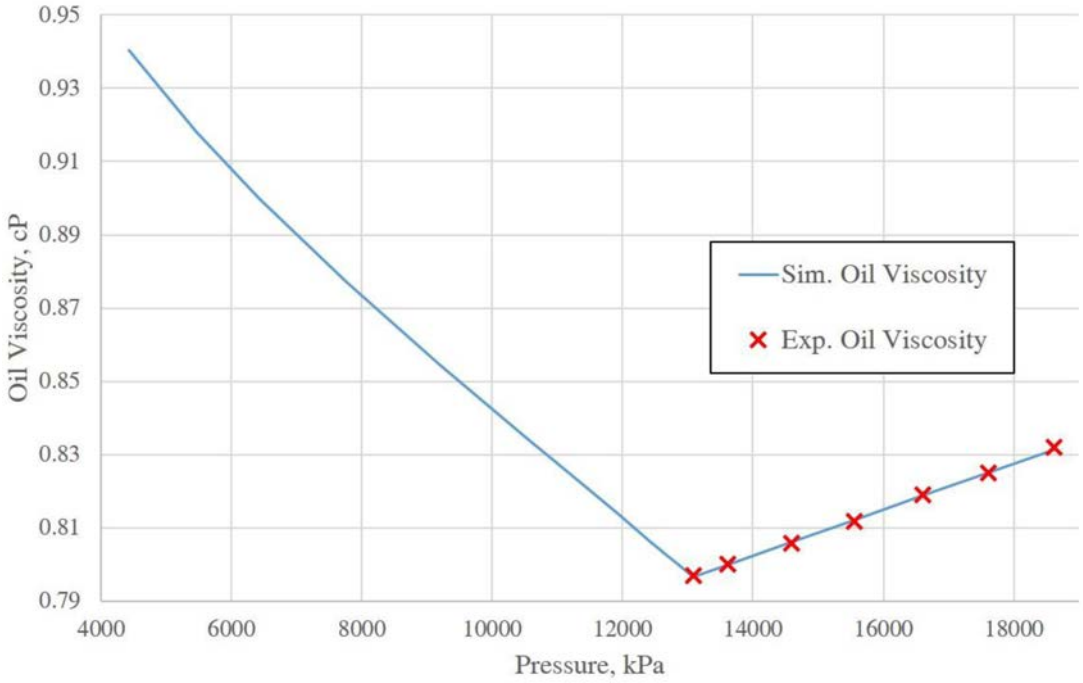

Figure. 7—Matched oil viscosity

The thermodynamic properties of the six components after tuning are summarized in Table 2. The binary interaction coefficients after tuning are listed in Table 3. It is worth mentioning that the binary interaction coefficients between any two pure components e.g., BIC between CH_4 and C_2H_6 were not tuned and default values from the WinProp library were used. The binary interaction coefficients between CO_2 (or N_2) and a pseudo-component e.g., BIC between CO_2 and C11+ might not be that reliable for modeling CO_2 (or N_2) injection due to its low molar fraction. We will be able to update the values as well as obtain a more accurate fluid model for gas injection if special experiments such as swelling test, or slim tube test are completed in the future.

Table 2—Thermodynamic properties of the eight components

Component	Molar fraction, %	Pc, atm	Tc, K	Acentric factor	MW, g/mol	Volume shift
CO_2	0.12	72.80	304.20	0.225	44.01	0
N_2	0.75	33.50	126.20	0.040	28.01	0
CH_4	31.72	45.40	190.60	0.009	16.04	0
C_2H_6	8.35	48.20	305.40	0.098	30.07	0
C_3H_8	9.70	41.90	369.80	0.152	44.10	0
C4-6	12.82	29.03	457.53	0.173	68.58	0
C7-10	12.86	21.87	463.77	0.354	118.75	-0.8696316
C11+	23.67	13.40	593.72	1.975	401.94	0.2376753

Downloaded from http://onepetro.org/SPEIOR/proceedings-pdf/20IOR/2-20IOR/D021S023R001/2369981/spe-200469-ms.pdf by Colorado School of Mines user on 12 September 2021

Table 3—Binary interaction coefficients between components

Component	CO_2	N_2	CH_4	C_2H_6	C_3H_8	C4-6	C7-10	C11+
CO_2	0	0	0.105	0.13	0.125	0.115	0.2	0.2
N_2	0	0	0.025	0.01	0.09	0.11	0.11	0.18
CH_4	0.105	0.025	0	2.689E-3	8.537E-3	8.711E-3	1.925E-2	4.054E-2
C_2H_6	0.13	0.01	2.689E-3	0	1.662E-3	4.623E-3	1.456E-2	3.746E-2
C_3H_8	0.125	0.09	8.537E-3	1.662E-3	0	1.366E-3	8.105E-3	2.685E-2
C4-6	0.115	0.11	8.711E-3	4.623E-3	1.366E-3	0	4.059E-3	2.333E-2
C7-10	0.2	0.11	1.925E-2	1.456E-2	8.105E-3	4.059E-3	0	8.119E-3
C11+	0.2	0.18	4.054E-2	3.746E-2	2.685E-2	2.333E-2	8.119E-3	0

Rock Properties

The average air permeability without confining pressure was estimated as 0.38 mD, which was used in benchmarking the geological model as well as the previous black oil models, making simulated BHP much higher than the actual BHP, as shown in Figure 3. Hence, we re-characterized the rock porosity and permeability with cores from well Y416 whose location is circled by the orange short dot line in Figure 1. Two 1.5 in (38.1 mm) diameter cores plugs were first cleaned by solvents (toluene, chloroform, and methanol sequentially) in a Soxhlet extractor and then dried in an oven. Then an automated unsteady-state permeability and porosity measurement instrument (Core Lab CMS-300) was used to measure the permeability and porosity under various confining stresses (Cho et al., 2013). The confining stress was gradually increased first (loading) and then reduced again (unloading). The results are summarized in Table 4 and Table 5 respectively. The porosity values from both cores are close to the initial average value of 12.1%. But the permeability measured under confining stress is two orders of magnitude smaller than the initial estimated value as 0.38 mD, which might explain the discrepancy between measured and simulated BHP in the previous model. Hence in the compositional submodel, a permeability multiplier as 0.01 was initially used during history matching.

Table 4—Permeability and porosity measured at different confining stress for core #1

Net confining stress, psi	Porosity, %	Permeability, 10^{-3} mD
788.7	12.30	2.03
1047.4	12.18	1.70
1514.7	12.05	1.34
1512.4	12.02	1.33
1106.1	12.10	1.45
857.1	12.16	1.55

Downloaded from http://onepetro.org/SPEIOR/proceedings-pdf/20IOR/2-20IOR/D021S023R001/2369981/spe-200469-ms.pdf by Colorado School of Mines user on 12 September 2021

Table 5—Permeability and porosity measured at different confining stress for core #2

Net confining stress, psi	Porosity, %	Permeability, 10^{-3} mD
735.8	13.64	6.22
985.8	14.12	5.40
1472.3	14.16	4.05
1550.5	14.17	3.91
1103.7	14.19	4.28
813.2	14.30	4.69

The unloading curves (upper two curves) are less stress-dependent than the loading curves (lower two curves) as shown in Figure 8. It was discussed by Zhu et al. (2018) that the first unloading process seems to better capture the stress-dependent behaviors especially for permeability than the first loading curve. Also, the hysteresis between loading and unloading curves will reduce and eventually vanish with more loading cycles (Teklu et al., 2016). Hence the unloading curve was used. Later, it was found that matrix permeability varied within the same order of magnitude would make a minor difference in simulation results.

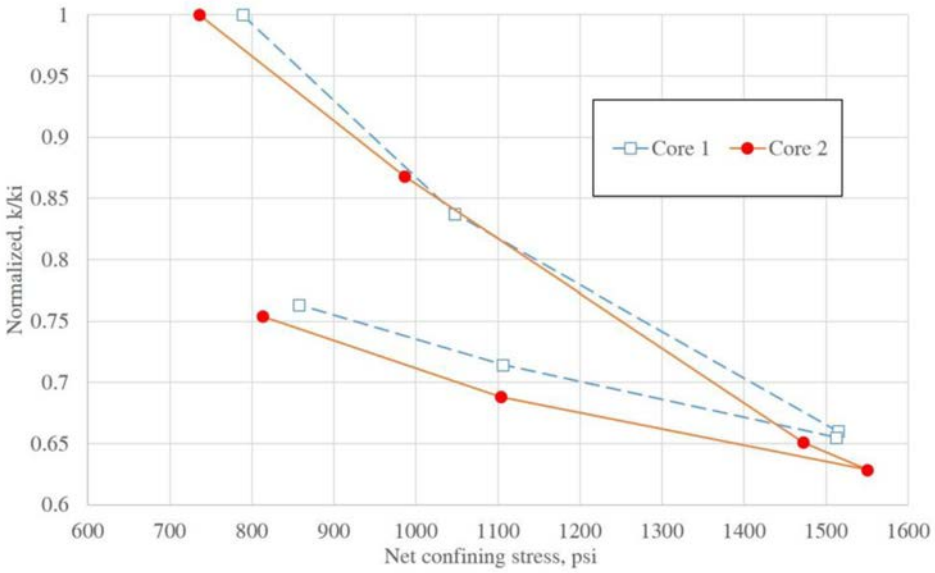

Figure. 8—Stress-dependent permeability measured from cores

Modeling of fracture network

To effectively model fracture networks, different approaches have been proposed, such as discrete fracture network mode (DFN), embedded discrete fracture model (EDFM), and continuum approach, such as dual-porosity or Multiple INteracting Continua (MINC). In this study, we choose the combination of dual-porosity model and local grid refinement (LGR) due to the usage of a commercial simulator.

Hydraulic fractures were modeled explicitly by LGR, and the grid containing HF has a width of 0.61 m, much larger than the actual width of HF as 0.002 m. The grid effective permeability is scaled accordingly to maintain the same fracture conductivity as specified (CMG, 2018). For example, the grid block effective permeability for the propped HF is 98.4 mD, which is the propped HF's conductivity (60 mD·m) divided by the grid width (0.61 m).

Nature fracture development for Chang 6_3 was well characterized in early studies (Zeng and Li, 2009; Liu, 2010; Liu et al., 2015). Despite the low initial oil rate for vertical wells, the fracture density was high

Downloaded from http://onepetro.org/SPEIOR/proceedings-pdf/20IOR/2-20IOR/D021S023R001/2369981/spe-200469-ms.pdf by Colorado School of Mines user on 12 September 2021

and fracture spacing was small as summarized in Table 6. In this study, natural fractures were modeled using a dual-porosity approach with fracture spacing set as 0.6 m in our base case. The natural fracture porosity was set as 0.001 to minimize the error introduced to pore volume after artificially adding fracture media into the previous single porosity model. And the intrinsic permeability of natural fracture was initialized as 10 mD, resulting in an effective nature fracture permeability as 0.01 mD.

Table 6—Nature fracture spacing (modified from Liu, 2010)

Well Name	NF spacing, m	Initial oil rate, m^3/d
Y284	0.3	1.79
Y414	0.4	3.41
Y286	0.5	0.56
Y411	0.7	0.23
Y287	1.3	0.47
Y293	1.4	1.32

Relative permeability and capillary pressure

The water-oil relative permeability curves for the matrix were based on the published data (Shi, 2012) and its endpoint values were calibrated during history matching as shown in Figure 9. Since the liquid-gas relative permeability curves were not available for this region, a hypothetical curve as shown in Figure 9 was used based on the data from published studies (Tian et al., 2019). The X-shape relative permeability curves were used for multiphase flow in fracture networks by assuming minimal residual saturation and negligible capillary pressure as shown in Figure 10

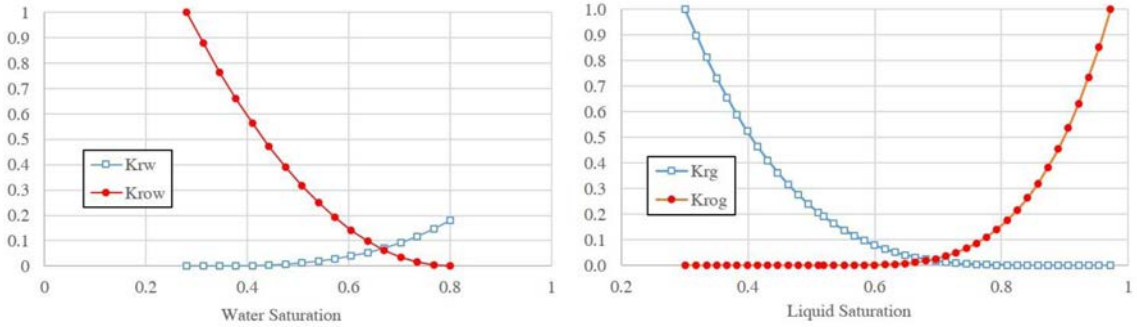

Figure. 9—The relative permeability curve for the matrix

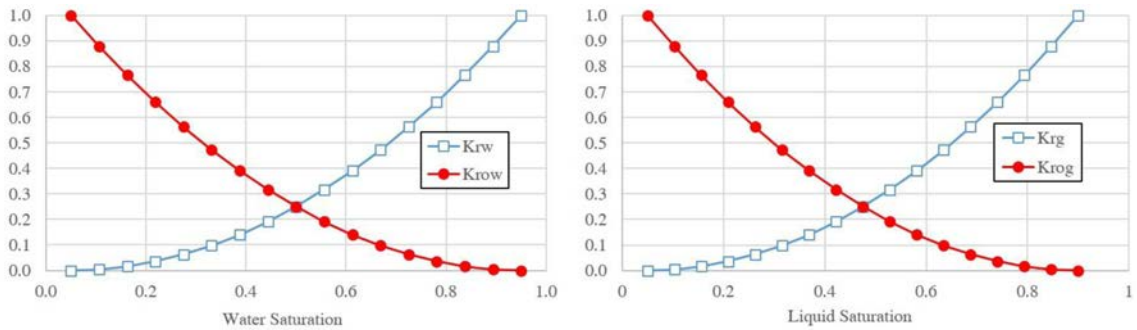

Figure. 10—The relative permeability curve for the fracture

Downloaded from http://onepetro.org/SPEIOR/proceedings-pdf/20IOR/2-20IOR/D021S023R001/2369981/spe-200469-ms.pdf by Colorado School of Mines user on 12 September 2021

The capillary pressure curve between air and mercury was available based on the experimental results of mercury injection by Shi (2012). The water-oil capillary curve was obtained by converting the mercury-air curve using the Leverett J-function. For example, to convert the mercury-air curve into the water-oil curve, we have,

$$P_{cow} = P_{cHg-air}\left(\frac{\gamma_{ow}\cos\theta_{ow}}{\gamma_{Hg-air}\cos\theta_{Hg-air}}\right)$$

The drainage curve between water and oil as shown in Figure 11 was used to initialize the water saturation at the beginning of the simulation.

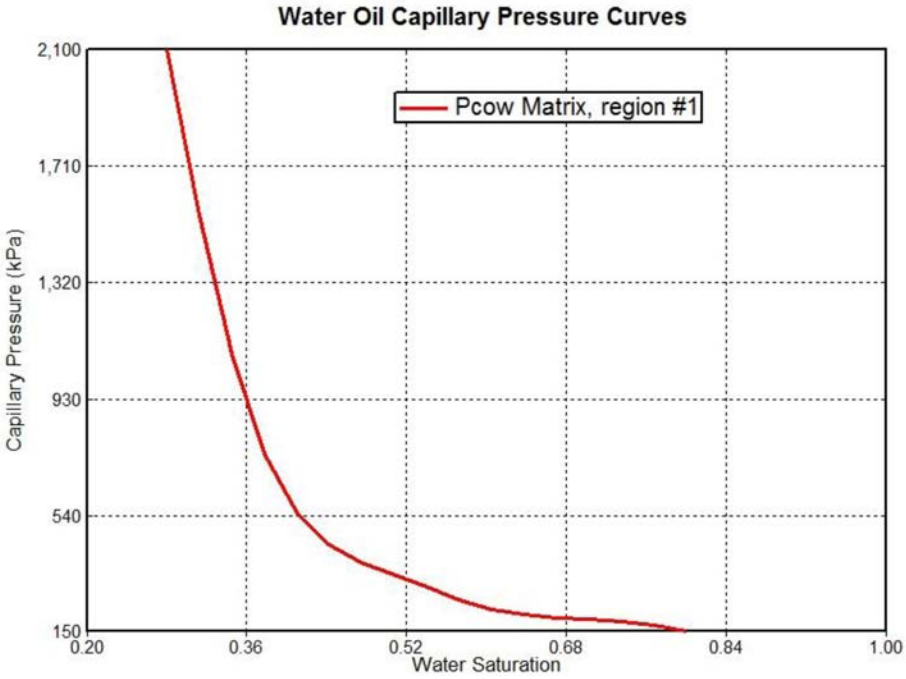

Figure. 11—Water-oil capillary pressure curve for the matrix

Currently, we are using the core flood and centrifuge to obtain a better characterization of rock-fluid data, such as relative permeability and capillary pressure curves. But for now, the data tuned after history matching will be used in this preliminary feasibility study.

History matching

The matching philosophy is to adjust a minimal number of parameters to fit the production data of well QP19. In order to match the BHP measured as 5.2 MPa from Aug 2016 to Sep 2016, the effective permeability of natural fractures was tuned to be 0.015 mD and the hydraulic fracture conductivity was adjusted from 60 mD·m to 64 mD·m. During history matching, the matrix permeability multiplier was initialized as 0.01 based on the abovementioned experimental studies but adjusting from 0.01 to 0.001 did not make significant impacts on simulation results, hence the initial value of 0.01 was retained.

To match the water cut, the relative permeability to water at residual oil saturation was reduced from 0.30 to 0.18. Despite mismatching oil rates at the early time of production (possibly due to unknown operational constraints), the history-matching performance as shown in Figure 12 was significantly improved compared with the previous black oil model shown in Figure 3 especially at the late time which is more influential on the succeeding gas huff-n-puff operations.

Downloaded from http://onepetro.org/SPEIOR/proceedings-pdf/20IOR/2-20IOR/D021S023R001/2369981/spe-200469-ms.pdf by Colorado School of Mines user on 12 September 2021

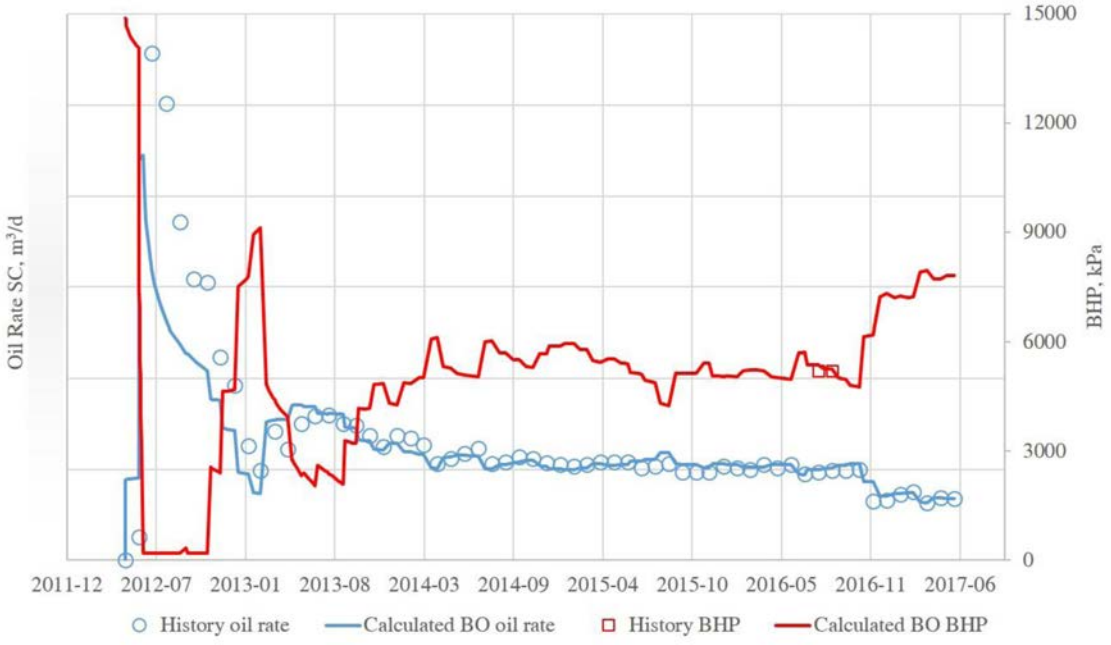

Figure. 12—Improved history-matching performance of Well QP19 by the current model

Sensitivity Analysis

Compositional effect of injectant

The composition of the injected gas is a key factor to the performance of huff-n-puff, which is one of the reasons using the compositional model rather than the black oil model for simulating gas injection. Hence, we simulated the scenarios with different injectant, including CH_4 (lean gas), produced gas (composition from the separator test), C_2H_6 (rich gas), and C_3H_8 (solvent). The composition of different injectant is s detailed in Table 7. The maximum injection BHP was set as 30 MPa as the minimum horizontal stress was estimated as 31.5 MPa from well Y290 whose location is circled by the red long dash line in Figure 1. The minimum miscibility pressure (MMP) between each injectant and reservoir oil was estimated by the multiple mixing cell method in WinProp. Due to the lack of data from the slim-tube or swelling test, its value might subject to inaccuracy. But its general trend qualitatively matched our expectation, i.e., the richer the gas, the lower the MMP.

Table 7—Composition of the injected gas

	Light			Intermediate			Heavy		MMP, MPa
	CO_2	N_2	CH_4	C_2H_6	C_3H_8	C4-6	C7-10	C11+	
Lean gas	0%	0%	100%	0%	0%	0%	0%	0%	27.0
	100%			0%			0%		
Produced gas	0.2%	1.3%	55.4%	14.3%	15.6%	12.5%	0.6%	0.0%	14.2
	57.0%			42.4%			0.6%		
Rich gas	0%	0%	0%	100%	0%	0%	0%	0%	6.9
	0%			100%			0%		
Solvent	0%	0%	0%	0%	100%	0%	0%	0%	3.5
	0%			100%			0%		

Downloaded from http://onepetro.org/SPEIOR/proceedings-pdf/20IOR/2-20IOR/D021S023R001/2369981/spe-200469-ms.pdf by Colorado School of Mines user on 12 September 2021

The compositional effect on the daily oil rate was shown in Figure 1. Injecting C_3H_8 achieved the best performance, increasing the cumulative oil production on the basis of waterflood by a factor of 2.28 after 5 cycles, then followed by C_2H_6 as 1.34, produced gas as 1.08. The improvement factor as shown on the right side of Figure 14, was calculated by dividing the cumulative C11+ production in moles after gas injection over the cumulative C11+ production in moles after waterflood. More generally, the improvement factor can be defined as the ratio of the cumulative oil production by an IOR/EOR method (gas huff-n-puff in this case) to the cumulative oil production following the original production scheme (waterflood in this case).This concept is more applicable in unconventional reservoirs (Hoffman, 2018; Zhang et al., 2019), as most of the oil in place outside SRV is not accessible, making the recovery factor in traditional sense very small.

A richer mixture (i.e. with higher molar fraction of intermediate component) will lead to a higher oil RF. Though C_3H_8 has the same value of intermediate fraction with C_2H_6, injecting C_3H_8 will still have a higher oil rate due to its lower MMP with the reservoir fluid than C_2H_6. Though lean gas (CH4) was injected above MMP, its oil recovery was even lower compared with the waterflood base case. This was because lean gas injection achieved miscibility at the injection front (middle or even the lower part of the reservoir because the horizontal well was completed at the top part of the reservoir). During production (puff stage) the miscibility front would not be produced efficiently as it might be far away from the wellbore or even return to immiscibility due to pressure drop. The original well completion was mainly designed to improve the sweep efficiency for waterflood by gravity, with water injectors placed at the bottom and producer at the top of the reservoir. However, such well placement may cause problems for gas huff-n-puff, especially for vaporizing gas drive which achieved miscibility at the leading front. But rich gas injection might mitigate such inherent flaws, which achieved miscibility at the injection tail.

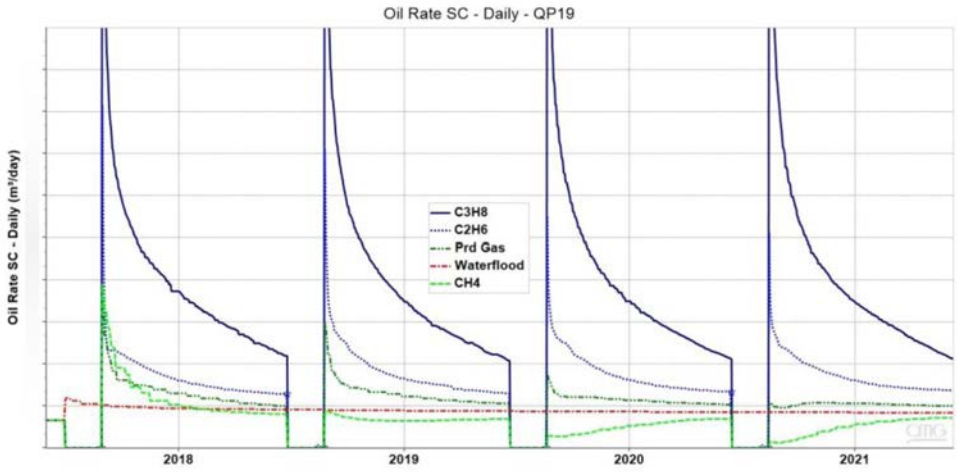

Figure. 13—Effect of the injectant's composition on oil rate

Downloaded from http://onepetro.org/SPEIOR/proceedings-pdf/20IOR/2-20IOR/D021S023R001/2369981/spe-200469-ms.pdf by Colorado School of Mines user on 12 September 2021

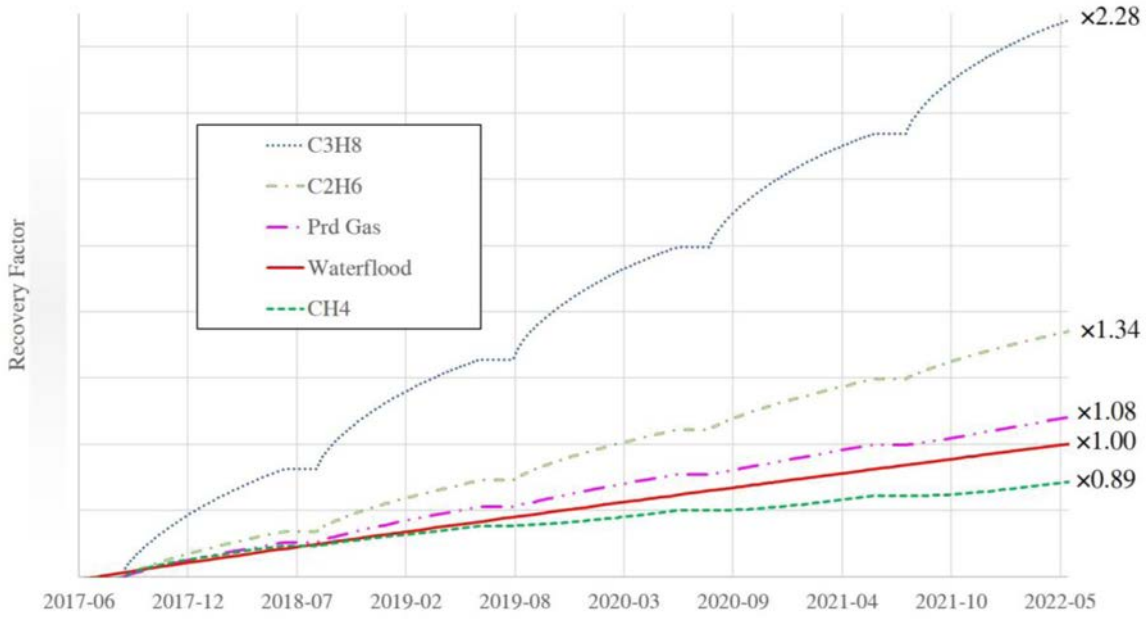

Figure. 14—Effect of the injectant's composition on cumulative C11+ production

Though injecting solvent (C_3H_8) or rich gas (C_2H_6) might result in a higher technical recovery factor compared with leaner gas, its economics might not be feasible. Hence, we proposed to mix the produced gas with either C_2H_6 or C_3H_8 to lower the gas cost. For example, with a mixing ratio of 60% C_3H_8 and 40% produced gas, we could still improve the cumulative C11+ production by a factor of 1.57 compared with waterflood base case, which was also higher than C_2H_6 injection as shown in Figure 15

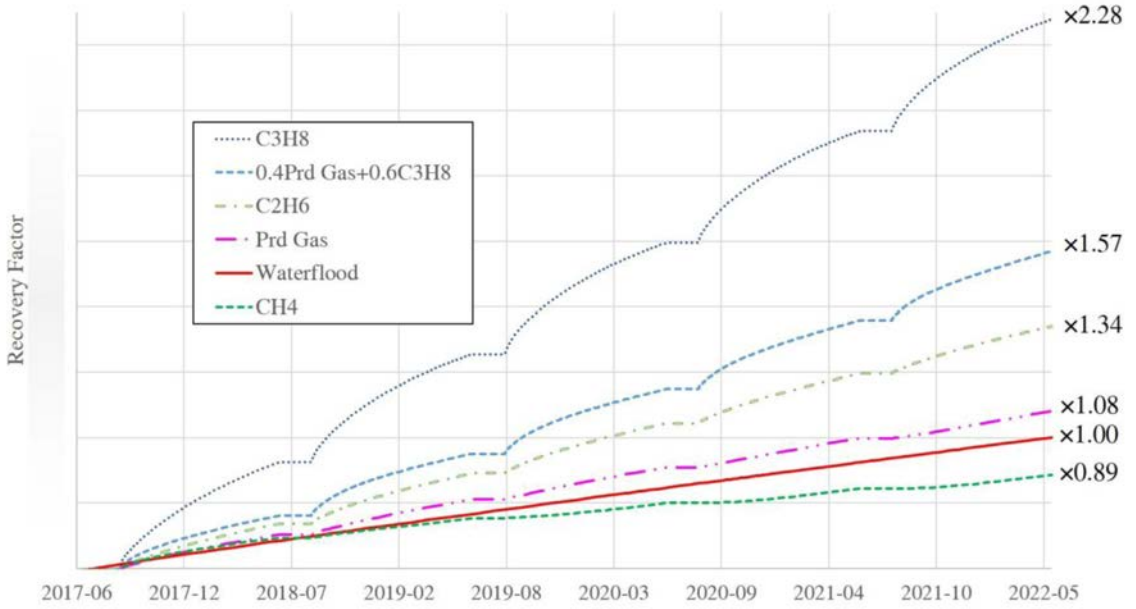

Figure. 15—Enrichment of produced gas with C_3H_8 outperforms C_2H_6 injection

Injection pressure

The BHP of the injection period is another important parameter influencing huff-n-puff performance. Often, the maximum BHP should be lower than the minimum horizontal stress to avoid undesired fracture propagation (Zhang et al., 2019) or possible gas channeling. Hence, we simulated three different maximum BHP for the injection period i.e., 20 MPa, 25 MPa, and 30 MPa. For example, during C_2H_6 injection, a

Downloaded from http://onepetro.org/SPEIOR/proceedings-pdf/20IOR/2-20IOR/D021S023R001/2369981/spe-200469-ms.pdf by Colorado School of Mines user on 12 September 2021

higher injection pressure would lead to a higher cumulative oil production as shown in Figure 16. This was consistent with the experimental studies (Abedini and Torabi, 2014; Song and Yang, 2017). But still injecting C_2H_6 at 30 MPa could not outperform the injection of C_3H_8 at 20 MPa. When injecting below 25 MPa, C_2H_6 would not lead to significant improvement compared with the waterflood base scenario.

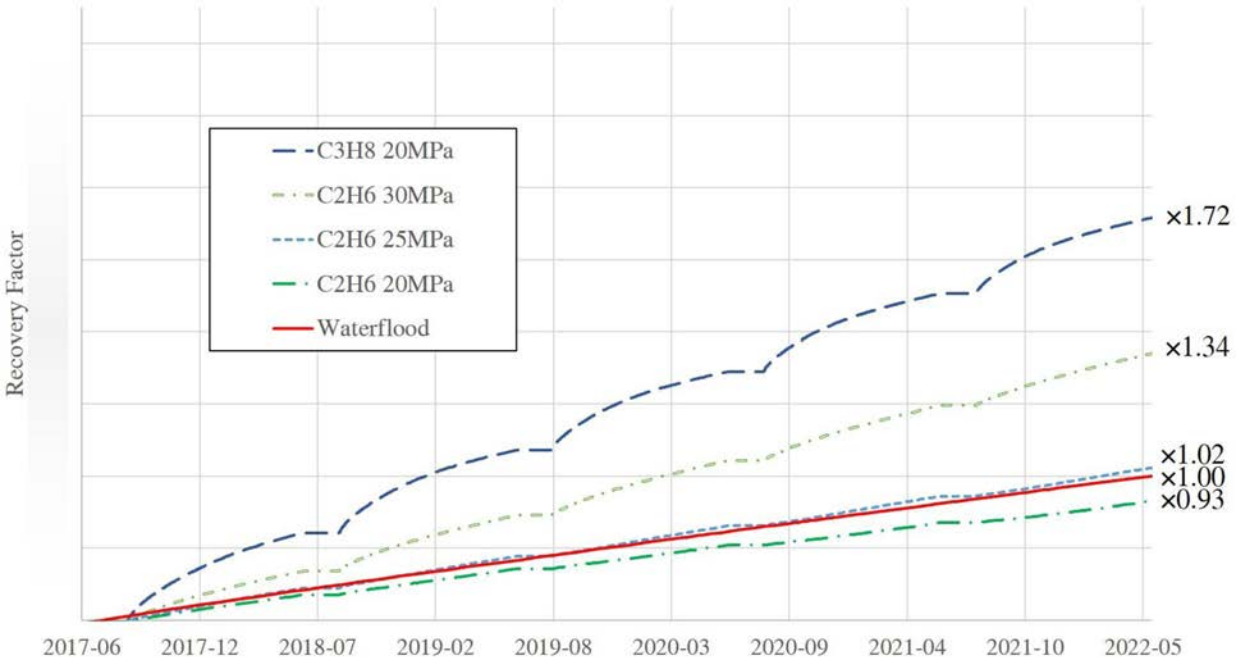

Figure. 16—Effect of injection pressure on rich gas (C_2H_6) injection

Injection of produced gas at 30 MPa could surpass the performance of injecting C_2H_6 at 25 MPa as shown in Figure 17, which is because the leaner composition of produced gas was compensated by a higher injection pressure when the richness difference of two injectant is not too large.

Downloaded from http://onepetro.org/SPEIOR/proceedings-pdf/20IOR/2-20IOR/D021S023R001/2369981/spe-200469-ms.pdf by Colorado School of Mines user on 12 September 2021

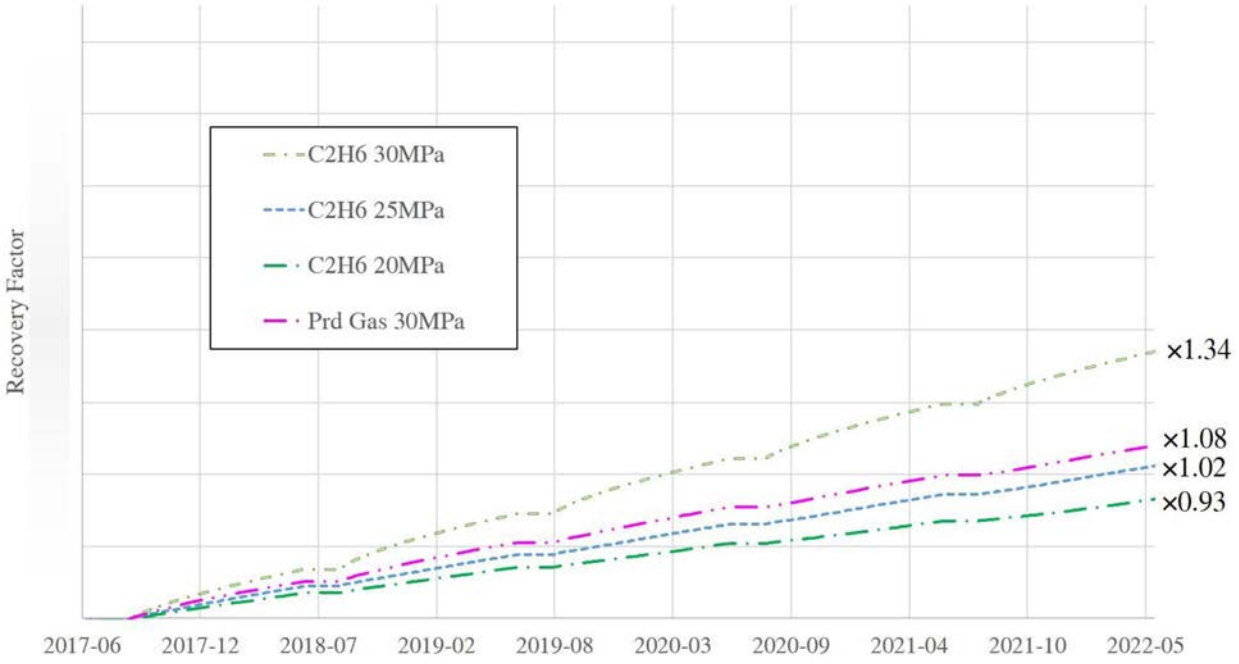

Figure. 17—Injecting produced gas at 30 MPa outperforms C_2H_6 injection at 25 MPa

Duration of the huff-n-puff stage

The duration of injection might affect the recovery factor. The huff-n-puff case above employed a scheme consisting of 50-day injection, 10-day soaking, and 300-day production. We then simulated different cases with 20-day, 70-day, 80-day, 90-day, and 110-day injection while maintaining the same soaking time and cycle duration constant as 360 days e.g., 80-day injection, 10-day soaking, and 270-day production. The simulation for 8 cycles shows that the cumulative C11+ production increased with injection time at first, but then the trend line would reach a plateau where increasing injection time would no longer lead to further improvement as shown in Figure 18. For C_2H_6 huff-n-puff at 30 MPa, the critical injection time was found to be 80 days.

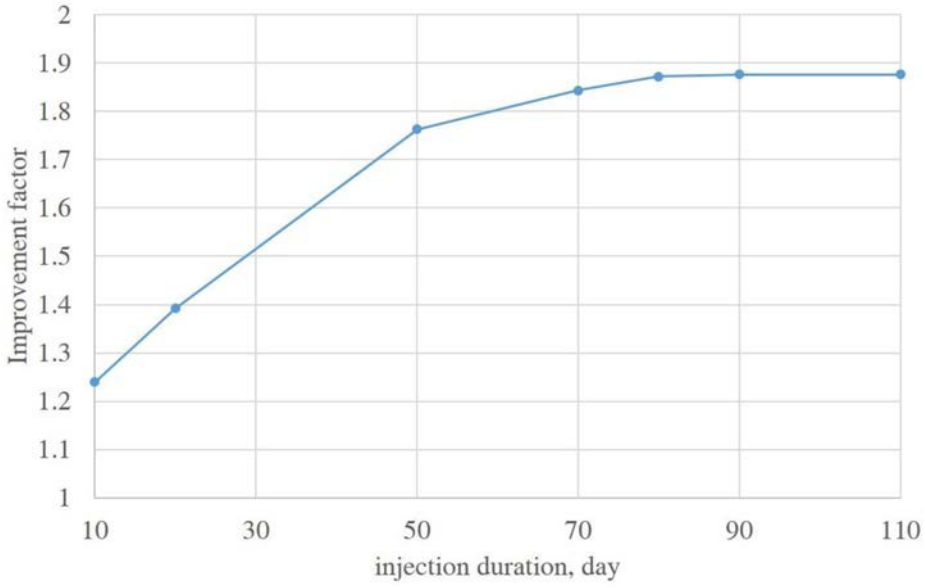

Figure. 18—Impact of injection duration per cycle on C_2H_6 huff-n-puff

Downloaded from http://onepetro.org/SPEIOR/proceedings-pdf/20IOR/2-20IOR/D021S023R001/2369981/spe-200469-ms.pdf by Colorado School of Mines user on 12 September 2021

Similarly, we investigated cases with different soaking time. The injection time was set the same as 80 days. The duration for one cycle was maintained the same as 360 days, e.g., 80-day injection 30-day soaking, 250-day production. The cumulative production has a relatively smaller dependence on soaking time compared with injection duration. At first, a longer soaking time would lead to a higher C11+ recovery, then a maximum would be achieved around 7-day as shown in Figure 19. After that, a longer soaking time would not increase but reduce C11+ recovery factor due to the possibility of losing miscibility or displacing the reservoir oil out of the SRV. For C_2H_6 huff-n-puff at 30 MPa, the optimal soaking time was found to be 7 days.

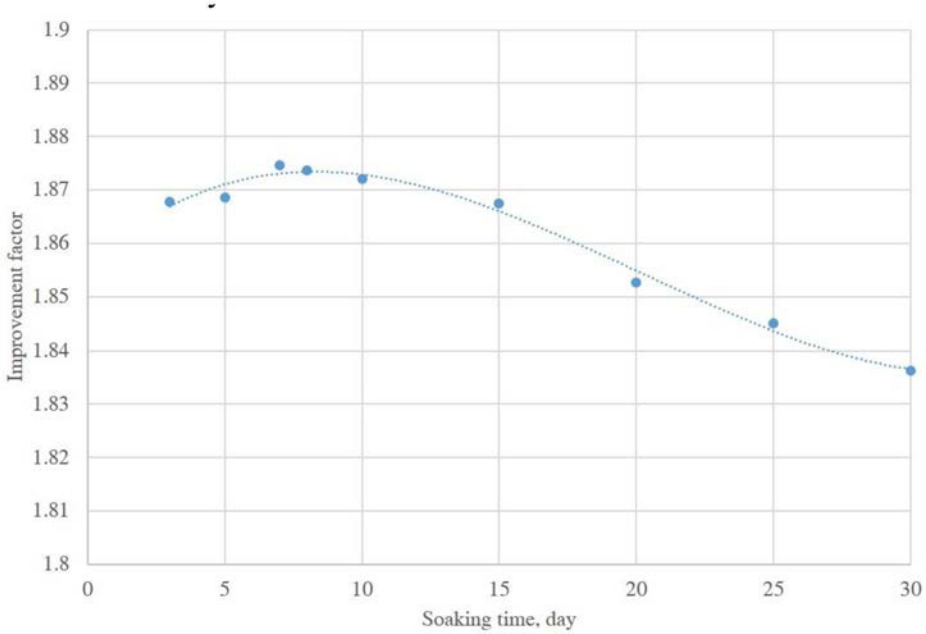

Figure. 19—Impact of soaking time per cycle on C_2H_6 huff-n-puff

Effect of fracture spacing

The properties of fracture network are known to influence the performance of reservoirs. Due to the inherent uncertainty regarding fracture spacing, different values of fracture spacing were investigated. Based on Table 6, we then investigated fracture spacing as 8 m, ∞ m (no fractures, single porosity model). Using a different fracture spacing other than the base case as 0.6 m would require re-history-matching the production data. We mainly re-tuned the natural fracture permeability to re-match the BHP. The water-oil relative permeability endpoint also was slightly tuned to match the water cut during waterflood. The conductivity and geometry for hydraulic fractures were kept the same as the base case. As shown in Figure 20, the recovery factor curves with different fracture spacings almost overlapped with each other after re-history-matching. The difference between natural fracture spacing as 0.6 m and 8 m after C_3H_8 huff-n-puff was almost negligible, which implies that as long as the BHP and water cut could match the historical data, huff-n-puff performance is insensitive to the uncertainties in fracture spacing. But the difference of dual porosity model and single porosity model was significant. The single porosity model though under the same injection pressure had a much lower recovery factor than the dual porosity model. C_3H_8 injection simulated by the single porosity model only showed a minor improvement on oil recovery, which was consistent with the published work (Carlsen et al., 2019). Physically, this was because dual porosity model would lead to a much higher interacting area between injected gas in fractures and stranding oil in the matrix.

Downloaded from http://onepetro.org/SPEIOR/proceedings-pdf/20IOR/2-20IOR/D021S023R001/2369981/spe-200469-ms.pdf by Colorado School of Mines user on 12 September 2021

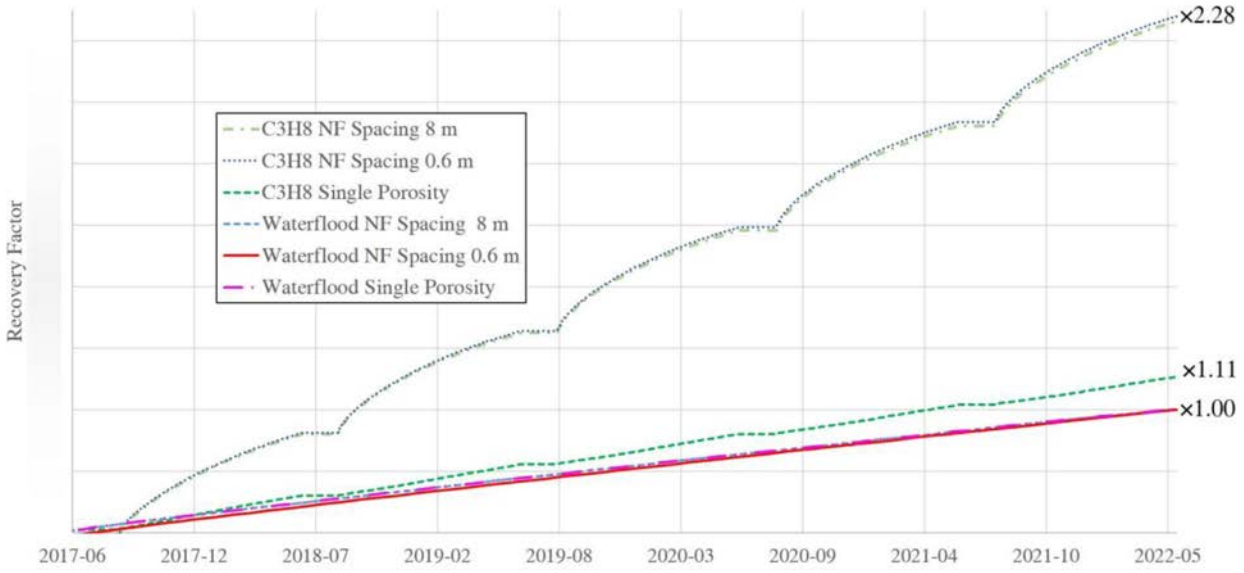

Figure. 20—Impact of fracture spacing on C_3H_8 huff-n-puff

Since the intensity of natural fractures in Y284 region was confirmed and quantified by previous fracture studies (Zeng and Li, 2009; Liu, 2010; Liu et al., 2015), the technical feasibility of injecting rich gas could be hence confirmed by the results of above simulations, which is less time-consuming and more economically affordable compared with core flood or field pilots. Though gas-oil relative permeability cannot be effectively tuned by production data of waterflood, it may potentially impact the gas injection process, which underscores the need for future investigation. The economic feasibility also needs to be addressed in the next phase of the research.

Conclusions

Ultra-low permeability Triassic formations, such as Chang 6_3, has become the new priority for developing the Ordos Basin. Due to the inefficiency of ongoing waterflood, we investigated the feasibility of gas huff-n-puff in Chang 6_3 using a compositional model. An eight-component fluid system was established to fit the experimental data. A typical well pattern was selected for compositional simulation, whose key inputs including relative permeability, fracture permeability, etc. were calibrated by matching the historical data. Huff-n-puff with lean gas (CH_4), produced gas, rich gas (C_2H_6), and solvent (C_3H_8) were simulated and compared with the current waterflood scenario.

1. Simulation results indicated that the richer the injected gas, the higher the oil recovery. C_3H_8 injection achieved the best performance, increasing the cumulative oil production by a factor of 2.3 after 5 cycles. Injecting C_2H_6 would improve RF by a factor of 1.34. Injecting produced gas would improve RF by a factor of 1.08.
2. Lean gas demonstrated a lower recovery factor than waterflood, because its MMP is close to the maximum allowable injection pressure, i.e., the minimum horizontal stress. Under current well placement design, the miscible oil bank, which forms at the injection front during vaporizing gas drive, would be displaced towards the reservoir bottom even out of the SRV, making lean gas injection ineffective.
3. However, the rich gas injection was compatible with such well placement design, as the miscible bank formed at the injection tail. Injecting produced gas enriched with C_3H_8 would achieve satisfactory performance, improving RF by a factor of 1.57 after 5 cycles.

Downloaded from http://onepetro.org/SPEIOR/proceedings-pdf/20IOR/2-20IOR/D021S023R001/2369981/spe-200469-ms.pdf by Colorado School of Mines user on 12 September 2021

4. The simulation also showed increasing injection pressure would also help increase the recovery factor. Moreover, the leaner composition could be compensated by higher injection pressure. The optimal injection duration and soaking time could also be obtained after sensitivity analysis.
5. Gas huff-n-puff performance was insensitive to the uncertainties in fracture spacing as long as the BHP and water cut could match the historical data. Using a single porosity model would show negligible incremental oil production in contrast to the dual-porosity model.
6. Based on the fracture spacing from the published work, we could verify the technical feasibility of rich gas injection in Chang 6_3 with the dual-porosity compositional simulation.

Acknowledgements

The authors thank Energi Simulation and Research Institute of Petroleum Exploration and Development (RIPED) for providing financial support to this study. Also, Computer Modelling Group (CMG) is acknowledged for the software license and support.

References

Abedini, A. and Torabi, F., 2014. Oil recovery performance of immiscible and miscible CO2 huff-and-puff processes. *Energy & Fuels*, **28** (2), pp.774–784.

Atan, S., Ajayi, A., Honarpour, M., Turek, E., Dillenbeck, E., Mock, C., Ahmadi, M. and Pereira, C., 2018, September. The viability of gas injection EOR in Eagle Ford shale reservoirs. In SPE Annual Technical Conference and Exhibition. Society of Petroleum Engineers.

Carlsen, M.L., Whitson, C.H., Dahouk, M.M., Younus, B., Yusra, I., Kerr, E., Nohavitza, J., Thuesen, M., Drozd, J.H., Ambrose, R. and Mydland, S., 2019, October. Compositional Tracking of a Huff-n-Puff Project in the Eagle Ford. In Unconventional Resources Technology Conference.

Cho, Y., Ozkan, E. and Apaydin, 0.G., 2013. Pressure-dependent natural-fracture permeability in shale and its effect on shale-gas well production. SPE Reservoir Evaluation & Engineering, **16** (02), pp.216–228.

CMG. 2018. GEM User's Guide. Computer Modeling Group.

Dong, Y., 2015. Evaluating of Development effects of Horizontal well in Yuan 284 Region, Huaqing oilfield (Master's thesis in Chinese, Xi'an Shiyou University).

Hoffman, B.T., 2018, March. Huff-N-Puff gas injection pilot projects in the eagle ford. In SPE Canada Unconventional Resources Conference. Society of Petroleum Engineers.

Hu, D., 2018. Study on optimization of combined imbibition and displacement development technology for ultralow permeability reservoir (Master's thesis in Chinese, China University of Petroleum).

Khan, S.A., 1992. An expert system to aid in compositional simulation of miscible gas flooding (Doctoral dissertation, University of Texas at Austin).

Liu, G., 2010. *Research on fracture developing characteristics of Chang63 reservoir*, Yangchang group in Huaqing area, Changqing petroleum field. (Master's thesis in Chinese, Lanzhou University)

Liu, G., Huang, C., Zhou, X., Zhang, L., and Pan, Y., 2015. Quantitative evaluation of fracture development in Triassic Yanchang Formation, Ordos Basin, NW China. *Petroleum Exploration and Development*, **42** (4), pp.486496.

Liu, X., Chang, Y., Lu, H., Chen, B., Li, J., Qi, Y. and Wang, C., 2012, January. Optimizing fracture stimulation in low-permeability oil reservoirs in the Ordos basin. In SPE Asia Pacific Oil and Gas Conference and Exhibition. Society of Petroleum Engineers.

Ran, X., 2013. Advanced Water Injection for Low Permeability Reservoirs: Theory and Practice. Gulf Professional Publishing.

Shangguan, Y., Zhang, Y. and Xiong, W., 2015. The effect of physical property changes on the water flooding development in Changqing oilfield Jurassic low permeability reservoir. *Petroleum*, **1** (4), pp.300–306.

Shi, T., 2012. The Study on the Micro-pore Structure and Percolation Characteristics of Yanchang Formation Chang6 Reservoir in Huaqing Area (Doctoral dissertation in Chinese, Northwest University).

Song, C. and Yang, D., 2017. Experimental and numerical evaluation of CO2 huff-n-puff processes in Bakken formation. *Fuel*, **190**, pp.145–162.

Teklu, T.W., Zhou, Z., Li, X. and Abass, H., 2016, June. Cyclic permeability and porosity hysteresis in mudrocks—experimental study. In 50th US Rock Mechanics/Geomechanics Symposium. American Rock Mechanics Association.

Tian, Y., Xiong, Y., Wang, L., Lei, Z., Zhang, Y., Yin, X., Wu, Y.S., 2019. A Compositional model for gas injection IOR/EOR in tight oil reservoirs under coupled nanopore confinement and geomechanics effects, Journal of Natural Gas Science and Engineering, **71**, pp.102973

Downloaded from http://onepetro.org/SPEIOR/proceedings-pdf/20IOR/2-20IOR/D021S023R001/2369981/spe-200469-ms.pdf by Colorado School of Mines user on 12 September 2021

Wang, L., Tian, Y., Yu, X., Wang, C., Yao, B., Wang, S., Winterfeld, P.H., Wang, X., Yang, Z., Wang, Y. and Cui, J., 2017. Advances in improved/enhanced oil recovery technologies for tight and shale reservoirs. *Fuel*, **210**, pp.425445.

Xin, Y., 2019. Evaluating of the effect of water injection development in Yuan 284 well area in Longdong area (Master's thesis in Chinese, Xi'an Shiyou University).

Yu, H., Yang, Z., Luo, L., Liu, J., Cheng, S., Qu, X., Lei, Q. and Lu, J., 2019. Application of cumulative-in-situ-injection-production technology to supplement hydrocarbon recovery among fractured tight oil reservoirs: A case study in Changqing Oilfield, China. *Fuel*, **242**, pp.804–818.

Zeng, L.B. and Li, X.Y., 2009. Fractures in sandstone reservoirs with ultra-low permeability: A case study of the Upper Triassic Yanchang Formation in the Ordos Basin, China. *AAPG Bulletin*, **93** (4), pp.461–477.

Zhang, C., Tian, Y., Shen, Y., Yao, B. and Wu, Y. S., 2019, October. Simulation of High Water-Cut in Tight Oil Reservoirs during Cyclic Gas Injection. In SPE Liquids-Rich Basins Conference-North America. Society of Petroleum Engineers.

Zhao, J., Fan, J., He, Y., Yang, Z., Gao, W., and Gao, W., 2015. Optimization of horizontal well injection-production parameters for ultra-low permeable—tight oil production: a case from Changqing Oilfield, Ordos Basin, NW China. *Petroleum Exploration and Development*, **42** (1), pp.74–82.

Zhu, S.Y., Du, Z.M., Li, C.L., Salmachi, A., Peng, X.L., Wang, C.W., Yue, P. and Deng, P., 2018. A semi-analytical model for pressure-dependent permeability of tight sandstone reservoirs. *Transport in Porous Media*, **122** (2), pp.235–252.

Downloaded from http://onepetro.org/SPEIOR/proceedings-pdf/20IOR/2-20IOR/D021S023R001/2369981/spe-200469-ms.pdf by Colorado School of Mines user on 12 September 2021